Structural and optoelectronic properties of lead-free $Cs_2InAgCl_6$, $Cs_2InAgBr_6$, Cs_2InAgI_6 double perovskites by density functional theory approach

MOJTABA MAHMOUDZADEH PIRVAHSHI[1,3], MORTEZA IZADIFARD[1,*], MOHAMMAD EBRAHIM GHAZI[1], NASSER SHAHTAHMASSEBI[2]
[1]*Faculty of Physics, Shahrood University of Technology, Shahrood, Iran*
[2]*Physics Department, Ferdowsi University of Mashhad, Mashhad, Iran*
[3]*Department of Science, Saravan Branch, Islamic Azad University, Saravan, Iran*

Using Density Functional Theory (DFT) within the Quantum ESPRESSO package, this study meticulously explores the structural and optoelectronic characteristics of lead-free $Cs_2InAgCl_6$, $Cs_2InAgBr_6$, and Cs_2InAgI_6 double perovskites. Stability assessments, grounded in Goldschmidt's tolerance and octahedral factors, confirm that all three compounds adopt stable cubic structures. Electronic band structure calculations employing both the Generalized Gradient Approximation (GGA) and the Heyd–Scuseria–Ernzerhof (HSE06) hybrid exchange-correlation functional reveal direct band gaps of approximately 3.16, 1.49, and 0.09 eV for $Cs_2InAgCl_6$, $Cs_2InAgBr_6$, and Cs_2InAgI_6, respectively. Notably, $Cs_2InAgCl_6$ and $Cs_2InAgBr_6$ exhibit significant optical absorption (~105 cm^{-1}) in the visible spectral range, underscoring their potential in optoelectronic and optical applications.

(Received September 9, 2024; accepted June 3, 2025)

Keywords: Cs_2InAgX_6, Halide Double-Perovskite, Band structure, Density-Functional Theory, Structural and Optical Properties, Dielectric Function

1. Introduction

AMX_3 organic-inorganic hybrid perovskite compounds, characterized by their direct band gaps of approximately 1.5 eV and their outstanding electronic and optical properties, have garnered significant attention from researchers. These compounds can incorporate $CH_3NH^+_3$ and Cs^+ cations in the A-site, with M representing a cation such as Pb^{+2}, and X constituting a halide anion (I^-, Br^-, Cl^-) [1-4]. Over the past decade, the power conversion efficiency (PCE) of perovskite photovoltaic cells utilizing these materials has witnessed a remarkable increase from 3.8% to 25.2% [4-6]. This enhancement underscores the substantial application potential of perovskite materials in diverse technologies, including photodetectors, lasers, photodiodes, and light-emitting diodes (LEDs) [5-10]. Despite the notable achievements of lead-based perovskites, they face significant challenges. The inherent instability of these compounds when exposed to moisture, light, and heat, coupled with the adverse environmental impacts of lead, poses considerable barriers to their development. In response, a concerted effort among researchers aims to identify and develop lead-free alternatives that exhibit comparable structural and functional attributes yet offer enhanced durability and reduced environmental impact [11-15]. In materials science, an innovative approach to eliminate lead involves substituting one monovalent B^+ cation and one trivalent C^{+3} cation for two divalent Pb^{2+} ions, thereby creating lead-free double perovskite structures. In these novel configurations, the M^{IV} position's cation maintains an equivalent total number of valence electrons to those found in traditional perovskite structures [16]. This strategic substitution not only paves the way for eliminating lead—a known environmental and health hazard—from the structures but also retains the desirable electronic characteristics of perovskites. The chemical versatility inherent to these double-perovskite structures affords the potential to engineer compounds that exhibit optimal optoelectronic properties coupled with enhanced stability. These quaternary materials are distinguished by their appropriate band gaps, commendable stability, superior light absorption capabilities, and distinctive properties, making them viable alternatives to lead-based perovskites [16-17]. Such advancements underscore the potential for these materials to revolutionize applications in photovoltaic cells and other optoelectronic devices, aligning with the ongoing quest for more sustainable and environmentally friendly alternatives in material science. In the intricate architecture of quaternary $A_2B^+C^{+3}X^{VII}_6$ double perovskites, a diverse array of elements can occupy each designated position, introducing a broad spectrum of potential material properties. Specifically, cations from group IA (Cs^+, Na^+, K^+, Rb^+) can be situated in the A^+ site, while group IB (Cu^+, Ag^+, Au^+) or group IIIA (In^+, Tl^+) elements can occupy the B^+ site. Similarly, the C^{+3} site can host Bi^{+3} or Sb^{+3}, and the halide site (X^-) can be replaced with a variety of anions, including F^-, Cl^-, Br^-, or I^-.

Recent advancements have led to the successful synthesis of $Cs_2AgBiCl_6$ and $Cs_2AgBiBr_6$ semiconductors,

which demonstrate remarkable stability when exposed to air and light. Such robustness makes them attractive as potential solar absorber materials. Nevertheless, the major drawback of $Cs_2AgBiCl_6$ and $Cs_2AgBiBr_6$ is their relatively large and indirect band gaps—generally exceeding 2 eV—significantly reducing their overall photovoltaic efficiency compared to conventional lead-based perovskites [17-21]. In an effort to mitigate this limitation, alternative double perovskites containing indium have been explored. For example, $Cs_2InSbCl_6$ is theorized to have a direct band gap ranging between 1.02 and 1.47 eV, while $Cs_2InBiCl_6$ has been predicted to exhibit a direct gap of about 0.91 to 1.68 eV. Such values are notably closer to the optimal range for solar absorption, potentially rivaling or even surpassing the performance of the well-known lead-based perovskite $CH_3NH_3PbI_3$. However, despite these promising theoretical predictions and their enticing band-gap characteristics, experimental realization of these compounds remains elusive, leaving a gap between theoretical promise and practical application [22-23]. This gap between theoretical potential and practical achievement underscores the ongoing challenges and opportunities within the field of material science, particularly in the development of lead-free, high-efficiency photovoltaic materials. The scholarly literature highlights that the distinctive optical and electronic properties of lead-based perovskite compounds are predominantly attributed to the unique $6s^2p^0$ electron configuration of lead (Pb). In the quest for alternative compositions, one promising strategy involves the substitution of Pb atoms with smaller inorganic cations, specifically targeting positions C^{+3} and B^{+}. Among these alternatives, the combination of indium (In) and silver (Ag) emerges as a compelling choice, facilitating the development of inorganic halide double perovskites that exhibit commendable stability. A notable exemplar of this innovative approach is $Cs_2InAgCl_6$, which is distinguished by a direct band gap of approximately 3.3 eV [23-26]. This material has garnered attention for its potential sensitization properties. The exploration of such alternatives not only helps circumvent environmental and health concerns associated with lead but also expands the repertoire of materials with tailored optical and electronic characteristics. The synthesis and characterization of compounds like $Cs_2InAgCl_6$ underscore the evolving landscape of perovskite research, emphasizing the pursuit of materials that balance performance with environmental stewardship.

This research paper presents a thorough Density Functional Theory (DFT) investigation, using the Quantum ESPRESSO package, of the structural, electronic, and optical properties of indium-based, lead-free halide double perovskites— $Cs_2InAgCl_6$, $Cs_2InAgBr_6$, and Cs_2InAgI_6. Distinguishing itself from existing literature, the study meticulously assesses the stability, electronic band structures, and optical properties of these compounds, revealing their direct band gaps and high absorption coefficients in the visible light spectrum. Unlike traditional AMX_3 perovskite compounds, which are hampered by toxicity and instability, the analyzed Cs_2InAgX_6 (X = Cl, Br, I) series offers a promising lead-free alternative with favorable band gaps, enhanced stability, strong light absorption and reduced environmental impact, aligning with the quest for sustainable material solutions in optoelectronics.

The novelty of this work lies in:

(i) Demonstrating an innovative approach to eliminating lead by substituting a monovalent and a trivalent cation with two divalent ions, thereby preserving desirable perovskite features while avoiding lead's detrimental effects;

(ii) Providing a detailed analysis of structural parameters and direct band-gap behavior for each halide variant;

(iii) Employing both the Generalized Gradient Approximation–Perdew–Burke–Ernzerhof (GGA–PBE) and the Heyd–Scuseria–Ernzerhof (HSE06) exchange-correlation functionals to obtain more accurate band-gap predictions;

(iv) Demonstrating significant optical absorption in the visible range, highlighting these materials' promise for photovoltaic and optoelectronic applications.

The meticulous analysis and direct comparison with previously published reports affirm the reliability of our DFT approach and establish a solid framework for future experimental validations. By thoroughly examining the Cs_2InAgX_6 series, this research advances the development of lead-free, high-efficiency photovoltaic materials.

2. Theoretical background

First-principles studies using the Quantum ESPRESSO package in the framework of density-functional theory (DFT), have been implied to investigate Cs_2InAgX_6 (X = Cl, Br, I) compounds. We used the Plane-wave self-consistent field (PWSCF) program to perform structural, electronic, and optical calculations [27-29]. We also applied face-centered cubic $Fm\bar{3}m$ elpasolite unit cell with rock-salt order for structural optimization. Cs: [Xe] $6s^1$ $6p^0$, In: [Kr] $4d^{10}$ $5s^2$ $5p^1$, Ag: [Kr] $4d^{10}$ $5s^1$, Cl: [Ne] $3s^2$ $3p^5$ and Br: [Ar] $3d^{10}$ $4s^2$ $4p^5$ were chosen as a configuration of valence electrons for each element in the applied pseudopotential. To find equilibrium structural parameters for each compound total energy minimization was performed. Kinetic energy cutoff of 480 eV for wave functions and 1920 eV for the charge density were chosen, respectively. The convergence threshold for self-consistent-field (SCF) 10^{-6} Ry and 10^{-4} Ry for forces was considered. Spin-orbit coupling (SOC) is also applied for electronic band structure, but its effect was insignificant. Structural and optical calculations were performed with GGA-PBE but for band gap estimation and band structure calculations, the Heyd-Scuseria-Ernzerhof (HSE06) hybrid function was used. The strategic use of GGA-PBE norm-conserving pseudopotentials, augmented with the HSE06 exchange-correlation functional, within the PWSCF

program of Quantum Espresso, is chosen for its balance between computational efficiency and accuracy in predicting structural and electronic properties of materials. This combination enhances the accuracy of band gap estimations—crucial for optoelectronic applications—while ensuring the study's findings on the structural, electronic, and optical characteristics of Cs_2InAgX_6 double perovskites are both reliable and comparable to existing research, facilitating advancements in the development of lead-free, high-efficiency photovoltaic materials. The validity of our method is comparable to the reported experimental and computational results of lattice constant and band gap values for these compounds. For atomic positions, lattice parameters, and cell volume optimization changes in total energies were set to be less than 0.1 meV/atom. In self-consistent structural calculations, we used a 6 × 6 × 6 Gamma-centered reciprocal space grid without a shift in k space, and also optical and band structure studies were performed with a denser 12 × 12 × 12 k-point grid. We also found that these systems with double perovskite symmetry examined in this study are non-magnetic.

3. Results and discussion

3.1. Structural analysis

As has been mentioned in the literature, we can predict the stability of perovskite compounds with two structural factors in the framework of the idealized solid-sphere model that has been used extensively. First Goldschmidt tolerance factor t_{eff} and second octahedral factor μ_{eff}. The appropriate range for t_{eff} should be 0.81 – 1.11 and for μ_{eff} must be within the range 0.44 - 0.90 to form a stable perovskite structure with cubic symmetry, according to previous reports [30]. In the current study for $Cs_2InAgCl_6$ (CIAC), $Cs_2InAgBr_6$ (CIAB), and Cs_2InAgI_6 (CIAI) double-perovskite compounds these parameters have been defined as below:

$$t_{eff}=(R_{Cs}+R_X)/\sqrt{2}\{(R_{In}+R_{Ag})/2+R_X\} \quad (1)$$

$$\mu_{eff}=(R_{In}+R_{Ag})/2R_X \quad (2)$$

R_{Cs}, R_{In}, R_{Ag}, and R_X are the ionic radii of Cs, In, Ag, and X (Cl, Br, I) ions, respectively, in these relations. Calculated values for t_{eff} and μ_{eff} are reported in Table 1. As shown from the reported data the obtained values for these factors are in the stable range for the examined compounds.

In Fig. 1, a double perovskite structure is shown. As we can see from the figure in the unit cell of face-centered cubic structure with rock-salt order and $Fm\bar{3}m$ space group, there is one $InCl/Br/I_6$ and one $AgCl/Br/I_6$ octahedron [31-33].

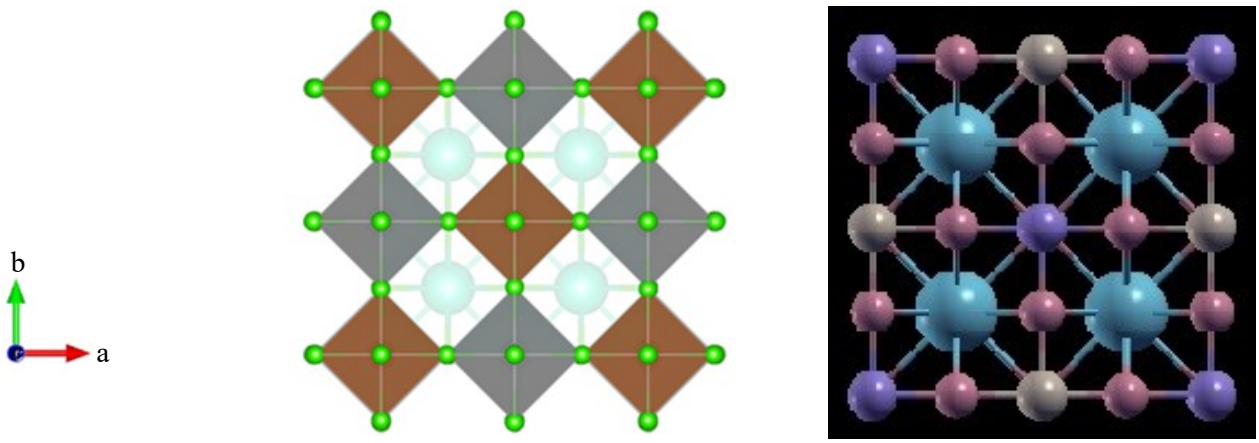

Fig. 1. Cubic structure of Cs_2InAgX_6 (X = Cl, Br, I) halide double perovskite compounds with $Fm\bar{3}m$ space group (colour online)

The Birch-Murnaghan equation of state was applied to optimize the lattice constant versus the total energy of the unit cell using the equation:

$$E(V)=E_0+\frac{9V_0B_0}{16}\{[(\frac{V_0}{V})^{\frac{2}{3}}-1]^2B_0+[(\frac{V_0}{V})^{\frac{2}{3}}-1]^2[6-4(\frac{V_0}{V})^{\frac{2}{3}}]\} \quad (3)$$

In this relation, E_o is minimum energy, B_o is the bulk modulus, and V_o is optimal volume. This energy minimization procedure for structural parameters was done at ambient pressure. The lattice constant a (Å), bulk modulus B_o (GPa), optimized volume V_o ($Å^3$), and its pressure derivatives B_p are reported in Table 1. The derivative of the bulk modulus concerning pressure plays an important role in determining the thermoplastic parameters of solids at high compression [34].

As can be seen from the data in the table, the values obtained for the lattice constant of the investigated structures are in remarkable agreement with the experimental and computational (DFT) reports of others. Also, an increase in the lattice constant from CIAC to CIAI occurs because of the increase in the radius of the halogen atom. Bulk modulus B_o and its pressure derivatives B_p, for CIAC, have a big difference with the other two compounds.

Table 1. The calculated and experimental structural parameters for CIAC, CIAB, and CIAI compounds

Sample	Pseudo type	t_{eff}	μ_{eff}	a (Å)	Reports		V_0 $(Å)^3$	B_0 (Gpa)	B_p
					Calculated	Exp.			
CIAC	PBE-NC	0.88	0.54	10.44	10.20[b], 10.43[a],10.62[b]	10.47[b,c]	283.53	126.7	12.08
CIAB	PBE-NC	0.87	0.51	11.08	10.74[b], 10.94[a]	-	340.12	25.5	4.44
CIAI	PBE-NC	0.86	0.45	11.82	11.52[b], 11.70[a]	-	413.74	21.3	4.45

[a][35], [b][24], [c][36]

3.2. Electronic band structure

The electronic properties were studied by examining the density of states and band structure. Calculated band structures with Fermi energy level set at zero and also density of states (DOS) of these compounds along the high symmetry lines in the Brillion-zone are depicted in Fig. 2. In^+ ions have the same fully occupied outmost s shells similar to Pb^{+2} so the band edge structure of these compounds is quite similar to those of $APbX^{VII}_3$ perovskites [36-38]. Also because of the absence of electronic symmetry reduction, both the valence band maximum (VBM) and conduction band minimum (CBM) are located at the zone center at Γ point so these compounds have a direct optical gap. Band gap values were obtained: 3.16 eV, 1.49 eV, and 0.09 for CIAC, CIAB, and CIAI structures. Calculated values for band gaps are reported in Table 1. As shown, the obtained values for investigated compounds agree with reported values for these structures in other literature.

Through the study of the partial density of states, the role of atomic orbitals at the edge of the conduction and valance bands was investigated. In Fig. 2 (right), these three compounds' partial atomic density of states (PDOS) is depicted. These figures show that the anti-bonding state of Cl/Br/I-p orbitals is more prominent at the VBM edge and due to the higher energy of In-s and Ag-s orbitals, the CBM is prominently composed of In-s, Ag-s, and also Cl/Br/I-p states. It can be seen that Cs^+ ions do not significantly contribute to the band edges. The effective mass of electrons is also calculated and reported in Table 2. A lower effective mass is indicative of high electron mobility, suggesting that electrons can move more freely and with less resistance through the material.

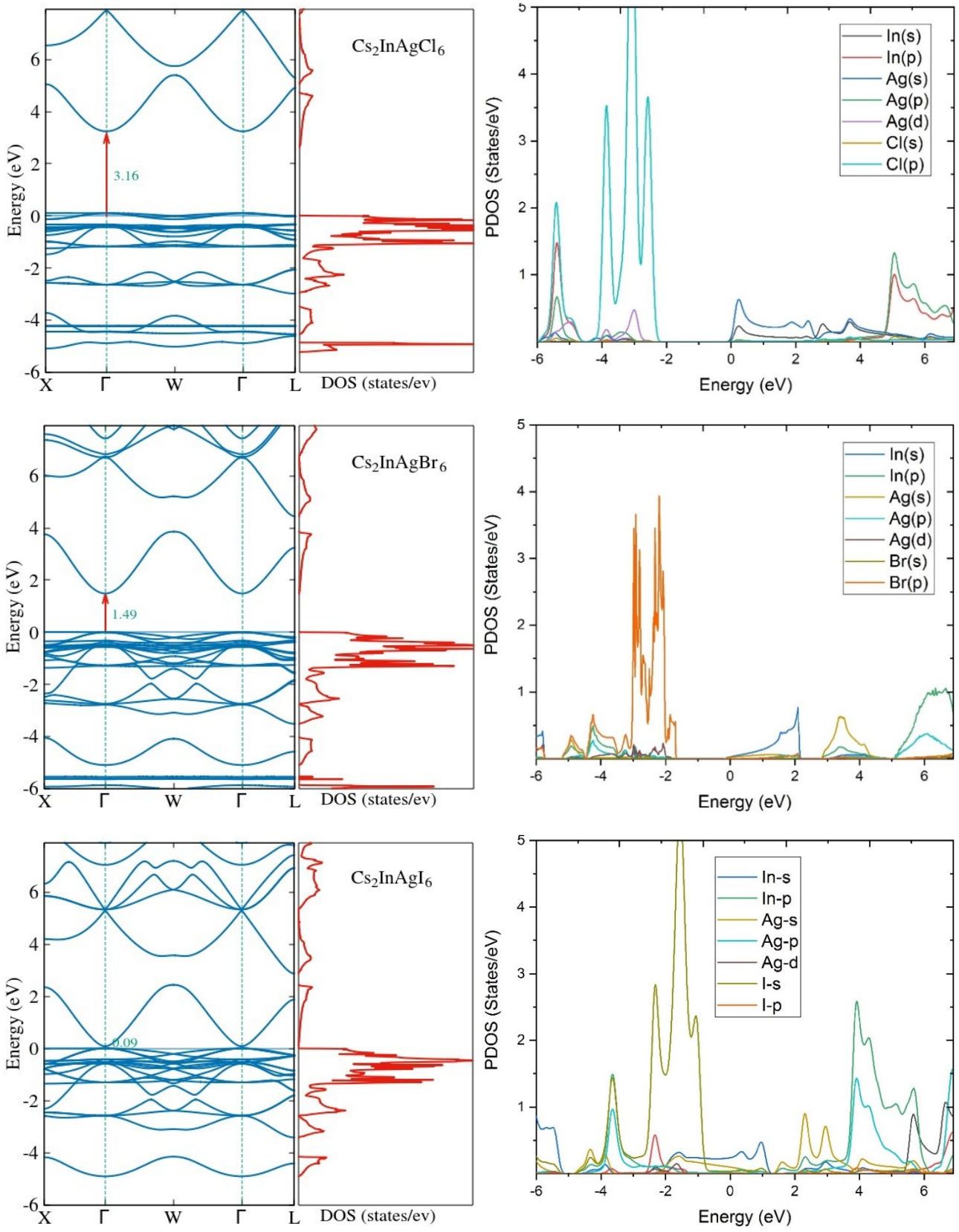

Fig. 2. Calculated electronic band structure and density of states (DOS) of CIAC, CIAB, and CIAI structures with HSE06 (the Fermi energy is set to be zero in band structure) (left) and partial density of states (PDOS) (right) (colour online)

Table 2. Calculated electronic and optical factors for $Cs_2InAgCl_6$ (CIAC), $Cs_2InAgBr_6$ (CIAB), and Cs_2InAgI_6 (CIAI) compounds

Compound	E_g(eV) (GGA)	E_g(eV) HSE06	Reported values	m^*/m_0	ε_0	Plasmon Frequency Energy (eV)	first $\boldsymbol{\varepsilon_r}$ peak
CIAC	2.12	3.16	2.49[a], 2.9[b], 3.2[c], 3.3[d]	0.43	2.38	7.93	4.22
CIAB	1.19	1.49	1.33[a], 1.38[b], 1.50[d]	0.48	3.64	7.42	4.12
CIAI	0	0.09	0.2[a]	-	-	-	-

[a][34], [b][24], [c][35], [d][23]

3.3. Optical calculations

The optical properties such as dielectric constants, absorption, reflection, and conductance Coefficients have a significant role in determining the applicability of these structures to optoelectronic components such as solar cell devices. These parameters can describe the properties of solids at microscopic and macroscopic levels. The Kramers-Kronig relation connects real and imaginary parts of the dielectric function. Therefore, through the study of the imaginary dielectric function with the help of Ehrenreich and Cohen's equation, important points about optical properties are obtained. According to this equation, the frequency-dependent complex dielectric function has two parts, real and imaginary, which are given by $\varepsilon(\omega) = \varepsilon_r(\omega) + i\varepsilon_i(\omega)$. This function describes the optical response of the medium to all photon energies [39]. The study of the imaginary part of the dielectric function, $\varepsilon_i(\omega)$, gives possible excitations between occupied and unoccupied states, and also the optical response of the medium can be determined. The imaginary part, $\varepsilon_i(\omega)$, obtained from the electronic structure calculation in the long-wavelength region, has been given by [39]:

$$\varepsilon_i(\omega)=\left(\frac{4\pi^2e^2}{m^2\omega^2}\right)\sum_{i,j}\int\langle i|M|j\rangle^2 f_i(1-f_i)d(E_f-E_i-\omega)d^3k \quad (4)$$

In this relation, M represents the dipole Matrix elements, i and j are the initial and final states, f_i is the Fermi distribution function for the state i, and E_i is the energy of an electron in the state i. From the Kramers - Kroning relation we can obtain $\varepsilon_r(\omega)$, the real part of the dielectric function, through the following equation [40]:

$$\varepsilon_r(\omega)=1+\frac{2}{\pi}P\int_0^{\infty}\frac{\omega'\varepsilon_i(\omega')d\omega'}{\omega'^2-\omega^2} \quad (5)$$

In this equation, P is the principal value of the integral. Fig. 3 shows the energy (frequency) dependence of the real and imaginary parts of dielectric constants for all compounds, calculated with GGA-PBE approximation. Because of the cubic symmetry of compounds, it was found that the optical dielectric tensor is isotropic.

However, due to the different values of the band gap, the absorption threshold in the diagrams is different. The real part (ε_r) describes the electron behavior in the band gap of matter. The graphs of ε_r show that the contribution of electrons in the static dielectric constant, $\varepsilon(0) = \varepsilon_\infty + \varepsilon_0$ is appreciably large, where ε_∞ (high-frequency dielectric constant or optical dielectric constant) and ε_0 (is due to the response of lattice vibrations) depict electronic and ionic contributions, respectively [41, 42].

Static dielectric constant [ε_0] related to the material behavior in low frequency or constant electric fields is changed with the material's band gap as it is clear from Fig. 3. The calculated values of ε_0 for these compounds are shown in Table 2. The first peak value of ε_r for CIAC occurs at 2.76 eV with a magnitude of 3.14 and for CIAB occurs at 1.46 eV with a magnitude of 4.12. The real part of dielectric function also explains electromagnetic wave dispersion when it penetrates a medium. It becomes negative in specific energy, which corresponds to plasma frequency. The energy that plasma frequency (the frequency above which $\varepsilon_r(\omega)$ becomes negative is likely to be a Drude-tail and the semiconductor starts to behave like a metal) occurs, has been reported in Table 2. Obtained values for CIAC, CIAB, and CIAI are 7.93, 7.42, and 5.86 respectively.

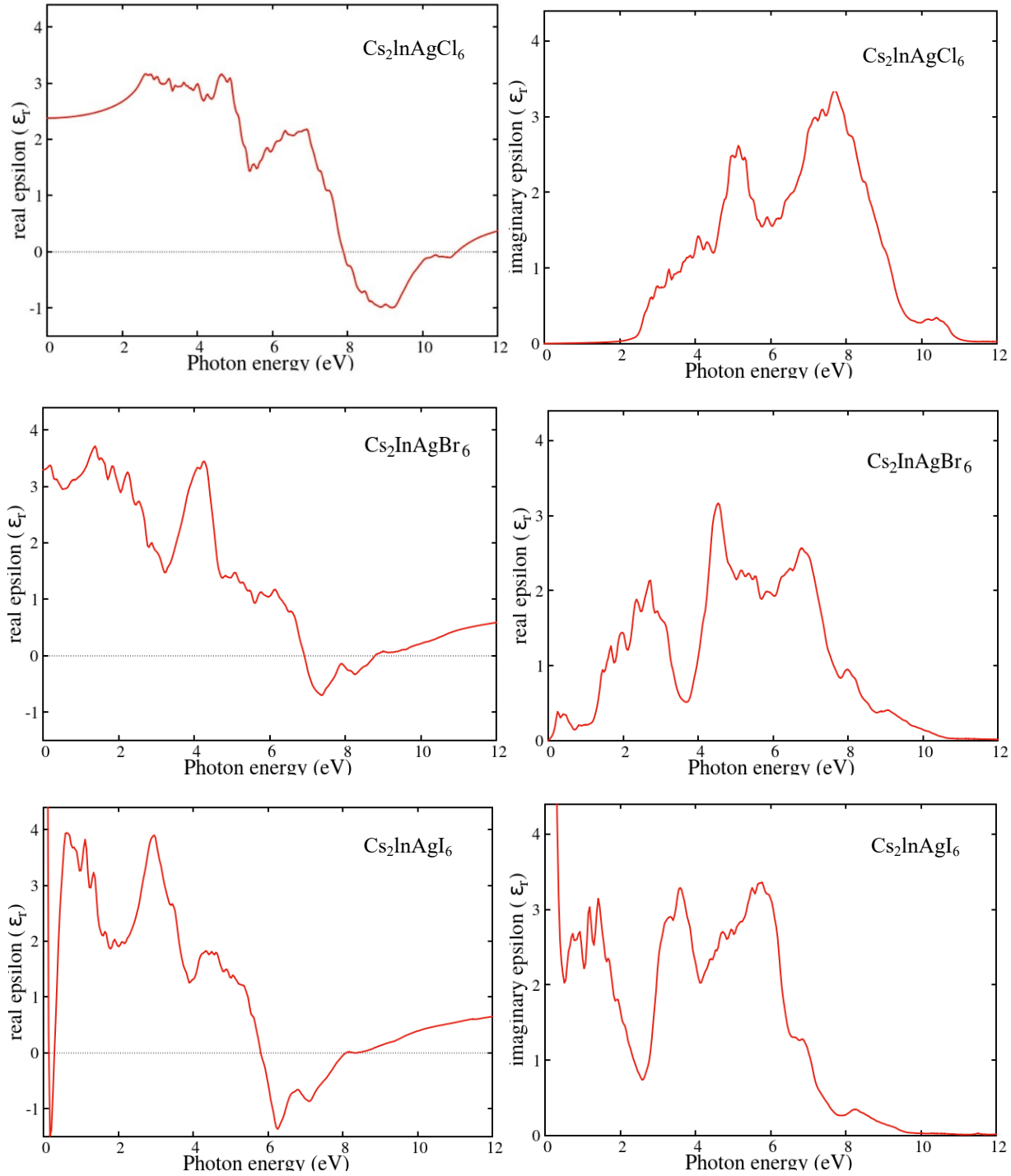

Fig. 3. The real and imaginary parts of the dielectric function for studied compounds are calculated with GGA-PBE approximation

There is a negative range in the $\varepsilon_r(\omega)$ spectrum. In this optical environment, the material loses its dielectric property and light is full so the semiconductor shows metallic behavior also the electric field of light can be screened with electrons around the surface before it gets into the bulk. For CIAC this negative range is from 7.93 to 10.96 eV, for CIBC is from 7.42 eV to 11.38 eV for CIAB and 5.84 to 7.92 eV for the CIAI compound.

An optical band gap can be obtained by considering the adjacent slope of the first local maximum (peak) of the imaginary part (ε_i) or the threshold energy, from the energy dependence of the imaginary part of the dielectric constant [42]. Threshold energy values in the spectra of $\varepsilon_i(\omega)$ for CIAC, CIBC, and CIAI are observed at 2.12, 1.14, and 0.07 eV which is near to the band gap values obtained with GGA-PBE approximation for each compound. The first peaks in the $\varepsilon_i(\omega)$ spectrum are related to the optical absorption and indicate the transition from the Cl/Br-p states of the VB to the unoccupied Cl/Br-p, s, and Ag-s states in the CB, which implies in the visible range [43].

In Fig. 4, investigated compounds' absorption and extinction coefficient spectra are indicated. The absorption edge for CIAC and CIAB lies in the visible range of spectra and is near the band gap of compounds.

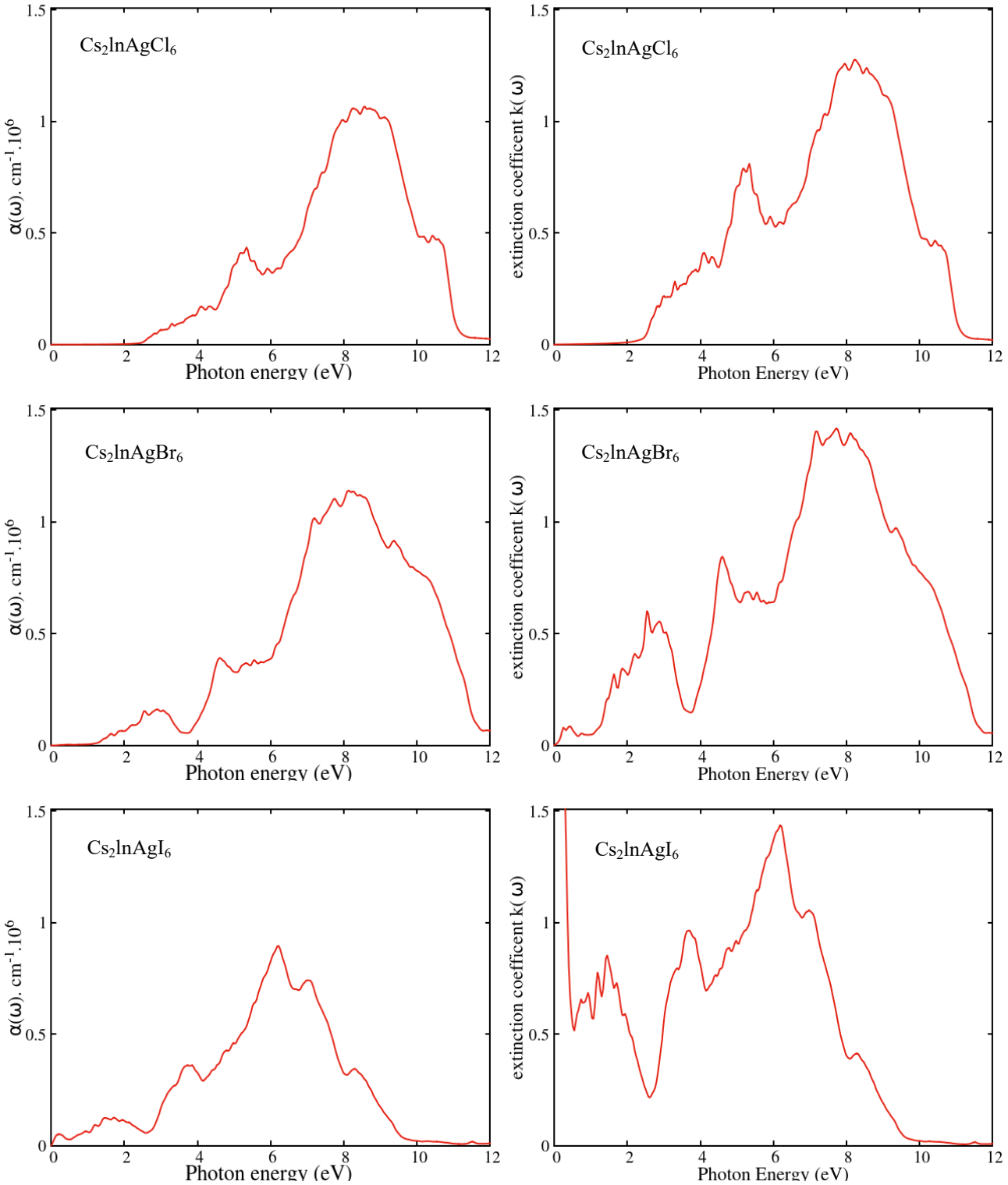

Fig. 4. Calculated absorption spectra and extinction coefficient spectra for studied compounds

As seen in the charts there is a strong absorption of photons (~10^5 cm^{-1}) in the range of 1.5 to 12.0 eV. This region represents the optically active area of these compounds. In this range, if the incoming photon energy is

equal to the electron energy difference between an occupied level and an unoccupied level, the electrons are excited and go to the unoccupied level of the conduction band. The absorption peak of CIAB is higher than CIAC and CIAI. These halide perovskite structures absorb almost all light in the visible and ultraviolet regions, which greatly increases their potential for use in optoelectronic industries [42]. But CIAB, because of the appropriate band gap value (1.49 eV) and the high absorption coefficient in the visible area (Comparable with CIAC and CIAI) can be a more suitable option. Also, corresponding diagrams of refractive index (n) and reflecting index (R) for investigated structures are depicted in Fig. 5.

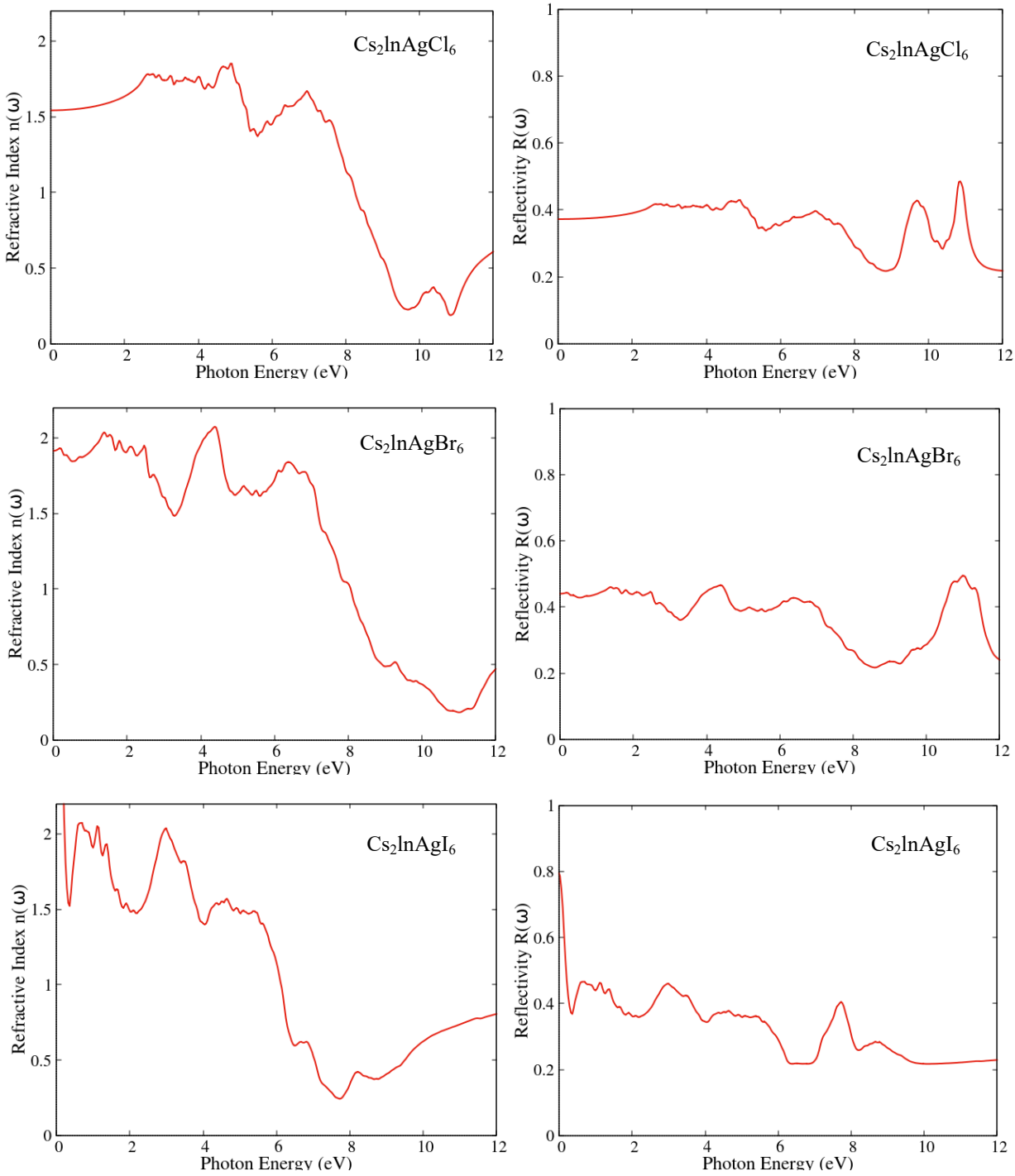

Fig. 5. The obtained refractive index (left) and reflective coefficient spectra (right) for studied compounds

As shown these structures have. So, high dielectric constants, high absorptions, and low reflectivity of CIAC and CIAB suggest that they can be used in a wide range of optoelectronic industries, including photovoltaic cells.

Also, CIAB can be a more suitable option due to the appropriate band gap value (1.49) and high absorption coefficient in the visible areas.

4. Conclusions

The structural and optoelectronic properties of lead-free halide double-perovskite compounds, specifically Cs_2InAgX_6 (where X represents Cl, Br, or I), were meticulously examined using the Plane-Wave Self-Consistent Field (PWSCF) program within the Quantum Espresso package. This investigation employed Generalized Gradient Approximation-Perdew, Burke, and Ernzerhof (GGA-PBE) norm-conserving pseudopotentials, augmented with the Heyd-Scuseria-Ernzerhof (HSE06) exchange-correlation functional for the density of states (DOS) and band structure analyses. The obtained structural and electronic parameters exhibit concordance with previously published reports, affirming the reliability of the computational approach. All three compounds under scrutiny demonstrated semiconductor behavior, with direct band gaps located at the Gamma point of the Brillouin zone. The band gap energies were quantitatively determined as 3.16 eV for $Cs_2InAgCl_6$ (CIAC), 1.49 eV for $Cs_2InAgBr_6$ (CIAB), and a notably lower value of 0.09 eV for Cs_2InAgI_6 (CIAI). Analysis of the density of states (DOS) and partial density of states (PDOS) revealed that the valence band maximum (VBM) edge states are predominantly composed of Cl/Br-p orbitals, whereas at the conduction band minimum (CBM) edge, In-s and Ag-s orbitals are significantly evident, with Cl/Br-p states also contributing to the CBM. Optical calculations further elucidated that these compounds exhibit strong absorption in the visible and ultraviolet regions, with an absorption coefficient of approximately 10^5 cm^{-1}. Such pronounced optical absorption capabilities, particularly for CIAC (with an energy gap Eg of 3.16 eV) and CIAB (Eg of 1.49 eV), underscore their potential utility in optoelectronics and optical devices. The findings from this study not only contribute to the understanding of the fundamental properties of these lead-free double-perovskite compounds but also highlight their prospective applications in developing high-efficiency optoelectronic devices.

References

[1] D. Gill, P. Bhumla, M. Kumar, S. Bhattacharya, Journal of Physics: Materials **4**(2), 025005 (2021).

[2] C. S. Liao, Q. Q. Zhao, Y. Q. Zhao, Z. L. Yu, H. Zhou, P. B. He, Jun-Liang Yang, M. Q. Cai, Journal of Physics and Chemistry of Solids **135**, 109060 (2019).

[3] M. I. Hossain, A. M. Hasan, W. Qarony, M. Shahiduzzaman, M. A. Islam, Y. Ishikawa, Yukiharu Uraoka, Nowshad Amin, Dietmar Knipp, Md. Akhtaruzzaman, Y. H. Tsang, Small Methods **4**(9), 2000454 (2020).

[4] A. Taya, P. Rani, J. Thakur, M. K. Kashyap, Vacuum **160**, 440 (2019).

[5] N. K. Tailor, M. Abdi-Jalebi, V. Gupta, H. Hu, M. I. Dar, G. Li, S. Satapathi, Journal of Materials Chemistry A **8**(41), 21356 (2020).

[6] M. M. Tavakoli, R. Tavakoli, Z. Nourbakhsh, A. Waleed, U. S. Virk, Z. Fan, Advanced Materials Interfaces **3**(11), 1500790 (2016).

[7] E. L. Lim, C. C. Yap, M. H. H. Jumali, M. A. M. Teridi, C. H. Teh, Nano-Micro Letters **10**, 1 (2018).

[8] D. Cui, Z. Yang, D. Yang, X. Ren, Y. Liu, Q. Wei, Haibo Fan, Jinghui Zeng, S. Liu, Journal of Physical Chemistry C **120**(1), 42 (2016).

[9] A. Al Mamun, T. T. Ava, H. J. Jeong, M. S. Jeong, G. Namkoong, Physical Chemistry Chemical Physics **19**(13), 9143 (2017).

[10] M. C. Jung, S. R. Raga, Y. Qi, RSC Advances **6**(4), 2819 (2016).

[11] P. Wang, Y. Wu, B. Cai, Q. Ma, X. Zheng, W. H. Zhang, Advanced Functional Materials **29**(47), 1807661(2019).

[12] P. V. Kamat, J. Bisquert, J. Buriak, ACS Energy Letters **2**(4), 904 (2017).

[13] M. Roknuzzaman, K. Ostrikov, H. Wang, A. Du, T. Tesfamichael, Scientific Reports **7**(1), 14025 (2017).

[14] A. Abate, Joule **1**(4), 659 (2017).

[15] F. Giustino, H. J. Snaith, ACS Energy Letters **1**(6), 1233 (2016).

[16] A. H. Slavney, T. Hu, A. M. Lindenberg, H. I. Karunadasa, Journal of the American Chemical Society **138**(7), 2138 (2016).

[17] C. N. Savory, A. Walsh, D. O. Scanlon, ACS Energy Letters **1**(5), 949 (2016).

[18] M. R. Filip, S. Hillman, A. A. Haghighirad, H. J. Snaith, F. Giustino, Journal of Physical Chemistry Letters **7**(13), 2579 (2016).

[19] E. T. McClure, M. R. Ball, W. Windl, P. M. Woodward, Chemistry of Materials **28**(5), 1348 (2016).

[20] J. Kangsabanik, V. Sugathan, A. Yadav, A. Yella, A. Alam, Physical Review Materials **2**(5), 055401 (2018).

[21] M. R. Filip, G. Volonakis, F. Giustino, Hybrid halide perovskites: fundamental theory and materials design. Handbook of Materials Modeling: Applications: Current and Emerging Materials, 295-324 (2020).

[22] M. M. Pirvahshi, M. Izadifard, M. E. Ghazi, Computational Condensed Matter **31**, e00669 (2022).

[23] Zhao, Xin-Gang, Ji-Hui Yang, Yuhao Fu, Dongwen Yang, Qiaoling Xu, Liping Yu, Su-Huai Wei, Lijun Zhang, Journal of the American Chemical Society **139**(7), 2630 (2017).

[24] George Volonakis, Marina R. Filip, Amir Abbas Haghighirad, Nobuya Sakai, Bernard Wenger, Henry J. Snaith, Feliciano Giustino, Journal of Physical Chemistry Letters **7**(7), 1254 (2016).

[25] Haque, Enamul, M. Anwar Hossain, Computational Condensed Matter **19**, e00374 (2019).

[26] P. Giannozzi, O. Andreussi, T. Brumme, O. Bunau, M. Buongiorno Nardelli, M. Calandra, R. Car, C.

Cavazzoni, D. Ceresoli, M. Cococcioni, N. Colonna, I. Carnimeo, A. Dal Corso, S. de Gironcoli, P. Delugas, R. A. DiStasio Jr, A. Ferretti, A. Floris, G. Fratesi, G. Fugallo, R. Gebauer, U. Gerstmann, F. Giustino, T. Gorni, J. Jia, M. Kawamura, H.-Y. Ko, A. Kokalj, E. Küçükbenli, M. Lazzeri, M. Marsili, N. Marzari, F. Mauri, N. L. Nguyen, H.-V. Nguyen, A. Otero-de-la-Roza, L. Paulatto, S. Poncé, D. Rocca, R. Sabatini, B. Santra, M. Schlipf, A. P. Seitsonen, A. Smogunov, I. Timrov, T. Thonhauser, P. Umari, N. Vast, X. Wu, S. Baroni, Journal of Physics: Condensed Matter **29**(46), 465901 (2017).

[27] Paolo Giannozzi, Stefano Baroni, Nicola Bonini, Matteo Calandra, Roberto Car, Carlo Cavazzoni, Davide Ceresoli, Guido L Chiarotti, Matteo Cococcioni, Ismaila Dabo, Andrea Dal Corso, Stefano de Gironcoli, Stefano Fabris, Guido Fratesi, Ralph Gebauer, Uwe Gerstmann, Christos Gougoussis, Anton Kokalj, Michele Lazzeri, Layla Martin-Samos, Nicola Marzari, Francesco Mauri, Riccardo Mazzarello, Stefano Paolini, Alfredo Pasquarello, Lorenzo Paulatto, Carlo Sbraccia, Sandro Scandolo, Gabriele Sclauzero, Ari P. Seitsonen, Alexander Smogunov, Paolo Umari, Renata M. Wentzcovitch, Journal of Physics: Condensed Matter **21**(39), 395502 (2009).

[28] Paolo Giannozzi, Oscar Baseggio, Pietro Bonfà, Davide Brunato, Roberto Car, Ivan Carnimeo, Carlo Cavazzoni, Stefano de Gironcoli, Pietro Delugas, Fabrizio Ferrari Ruffino, Andrea Ferretti, Nicola Marzari, Iurii Timrov, Andrea Urru, Stefano Baroni, Journal of Chemical Physics **152**(15), 154105 (2020).

[29] Edson Meyer, Dorcas Mutukwa, Nyengerai Zingwe, Raymond Taziwa, Metals **8**(9), 667 (2018).

[30] Zhao, Xin-Gang, Dongwen Yang, Ji-Chang Ren, Yuanhui Sun, Zewen Xiao, Lijun Zhang, Joule **2**(9), 1662 (2018).

[31] A. H. Slavney, T. Hu, A. M. Lindenberg, H. I. Karunadasa, J. Am. Chem. Soc. **138**, 2138 (2016).

[32] Femi Igbari, Zhao-Kui Wang, Liang-Sheng Liao, Advanced Energy Materials **9**(12), 1803150 (2019).

[33] M. Hebbache, M. Zemzemi, Physical Review B **70**(22), 224107 (2004).

[34] Manaf A. Mahammed, Hamsa B. Mohammed, Advances in Condensed Matter Physics **2023**(1), 9518475 (2023).

[35] Fatima Aslam, B. Sabir, M. Hassan, Applied Physics A **127**(2), 1 (2021).

[36] Jiajun Luo, Shunran Li, Haodi Wu, Ying Zhou, Yang Li, Jing Liu, Jinghui Li, Fei Yi, Guangda Niu, Jiang Tang, ACS Photonics **5**(2), 398 (2018).

[37] Wan-Jian Yin, Tingting Shi, Yanfa Yan, Advanced Materials **26**(27), 4653 (2014).

[38] Wan-Jian Yin, Ji-Hui Yang, Joongoo Kang, Yanfa Yan, Su-Huai Wei, Journal of Materials Chemistry A **3**(17), 8926 (2015).

[39] FengHui Tian, ChengBu Liu, Journal of Physical Chemistry B **110**(36), 17866 (2006).

[40] Junli Chang, Hong Chen, Guangzhao Wang, Biao Wang, Xiaorui Chen, Hongkuan Yuan, RSC Advances **9**(12), 7015 (2019).

[41] Sheikha Lardhi, Dalal Noureldine, Moussab Harb, Ahmed Ziani, Luigi Cavallo, Kazuhiro Takanabe, Journal of Chemical Physics **144**(13), 134702 (2016).

[42] Md Roknuzzaman, Chunmei Zhang, Kostya Ken Ostrikov, Aijun Du, Hongxia Wang, Lianzhou Wang, Tuquabo Tesfamichael, Scientific Reports **9**(1), 1 (2019).

[43] Masaki Shirayama, Hideyuki Kadowaki, Tetsuhiko Miyadera, Takeshi Sugita, Masato Tamakoshi, Masato Kato, Takemasa Fujiseki, Daisuke Murata, Shoto Hara, Takurou N. Murakami, Shohei Fujimoto, Masayuki Chikamatsu, Hiroyuki Fujiwara, Physical Review Applied **5**(1), 014012 (2016).

*Corresponding author: mizadifard@shahroodut.ac.ir